

Computational Modeling of Dapsone Interaction With Dihydropteroate Synthase in *Mycobacterium leprae*; Insights Into Molecular Basis of Dapsone Resistance in Leprosy

Sundeep Chaitanya V.,^{1*} Madhusmita Das,¹ Pritesh Bhat,² and Mannam Ebenezer³

¹Research Officer, Department of Laboratories, Molecular Biology and Immunology Division, The Schieffelin Institute of Health-Research and Leprosy Center (SIH-R&LC), Karigiri, Vellore, Tamil Nadu 632106, India

²Applications Scientist, Schrodinger, Inc., Near KMVA Vidya Niketan, Mahalakshimpuram, Bangalore 560 086, India

³The Schieffelin Institute of Health-Research and Leprosy Center (SIH-R&LC), Karigiri, Vellore, Tamil Nadu 632106, India

ABSTRACT

The molecular basis for determination of resistance to anti-leprosy drugs is the presence of point mutations within the genes of *Mycobacterium leprae* (*M. leprae*) that encode active drug targets. The downstream structural and functional implications of these point mutations on drug targets were scarcely studied. In this study, we utilized computational tools to develop native and mutant protein models for 5 point mutations at codon positions 53 and 55 in 6-hydroxymethyl-7, 8-dihydropteroate synthase (DHPS) of *M. leprae*, an active target for dapsone encoded by *folp1* gene, that confer resistance to dapsone. Molecular docking was performed to identify variations in dapsone interaction with mutant DHPS in terms of hydrogen bonding, hydrophobic interactions, and energy changes. Schrodinger Suite 2014-3 was used to build homology models and in performing molecular docking. An increase in volume of the binding cavities of mutant structures was noted when compared to native form indicating a weakening in interaction (60.7 Å³ in native vs. 233.6 Å³ in Thr53Ala, 659.9 Å³ in Thr53Ile, 400 Å³ for Thr53Val, 385 Å³ for Pro55Arg, and 210 Å³ for Pro55Leu). This was also reflected by changes in hydrogen bonds and decrease in hydrophobic interactions in the mutant models. The total binding energy (ΔG) decreased significantly in mutant forms when compared to the native form (−51.92 Kcal/mol for native vs. −35.64, −35.24, −46.47, −47.69, and −41.36 Kcal/mol for mutations Thr53Ala, Thr53Ile, Thr53Val, Pro55Arg, and Pro55Leu, respectively). In brief, this analysis provided structural and mechanistic insights to the degree of dapsone resistance contributed by each of these DHPS mutants in leprosy. *J. Cell. Biochem.* 116: 2293–2303, 2015. © 2015 Wiley Periodicals, Inc.

KEY WORDS: DIHYDROPTEROATE SYNTHASE; DAPSONE; DRUG RESISTANCE; MULTIDRUG THERAPY; POINT MUTATIONS; MOLECULAR DOCKING; BINDING AFFINITIES

Leprosy, a chronic infectious disease, is caused by an obligate intracellular pathogen- *Mycobacterium leprae* (*M. leprae*). Although the prevalence of this disease has significantly decreased after the introduction of WHO regimen of multi-drug therapy (MDT), the incidence remains high with approximately 232,857 cases reported globally in 2013 out of which 134,752 cases were reported from India [WHO, 2014]. Dapsone has been used in the treatment of leprosy since 1945 [Zhu and Stiller, 2001]. Due to the emergence and

spread of dapsone-resistant *M. leprae* from 1976 [Friedmann, 1973], WHO recommended and implemented control measure for leprosy with MDT, with the inclusion of rifampin in 1985 [Bullock, 1983] and ofloxacin in 1996 as a second line antibiotic [Ji and Grosset, 1991]. In India, the prevalence rate for leprosy before the initiation of MDT was 24/10,000 population. With the introduction of MDT, this figure was reduced to less than 1/10,000 population in the year 2005 [Desikan, 2012]. There is inadequate understanding on the modes of

Conflict of interest: The authors declare that they do not have any conflict of interest.

*Correspondence to: Mr. Sundeep Chaitanya V., MSc (PhD), Research Officer, Department of Laboratories, Molecular Biology and Immunology Division, The Schieffelin Institute of Health-Research and Leprosy Center (SIH-R&LC), Karigiri, Vellore, Tamil Nadu 632106, India. E-mail: sundeepchaitanya@gmail.com

Manuscript Received: 26 February 2015; Manuscript Accepted: 31 March 2015

Accepted manuscript online in Wiley Online Library (wileyonlinelibrary.com): 2 April 2015

DOI 10.1002/jcb.25180 • © 2015 Wiley Periodicals, Inc.

entry, gene regulation, metabolism, and survival of *M. leprae* in the host. Additionally, there is a risk that drug resistant strains of *M. leprae* could emerge in endemic countries and without an understanding of the biology of this organism, there is a possibility of resurgence of this disease with drug resistant strains.

Dapsone (4, 4'-diaminodiphenylsulfone) inhibits the bacterial dihydrofolic acid synthesis by binding to the active site on 6-hydroxymethyl-7, 8-dihydropteroate synthase (DHPS), an enzyme involved in the condensation of para-aminobenzoic acid (pABA) with 6-hydroxymethyl-7, 8-dihydropterin-pyrophosphate to form 7, 8-dihydropteroate and pyrophosphate [Zhu and Stillier, 2001]. Dapsone competes with para-aminobenzoate on the active site of DHPS and inhibits the bacterial dihydrofolic acid synthesis. Owing to the absence of this enzyme in eukaryotes, it was chosen as one of the suitable drug targets for interaction with sulfonamides and sulfones which are structural analogues of pABA [Jk et al., 1980]. The crystal structure of prokaryotic DHPS is a homodimer and in *Mycobacterium tuberculosis* (*M. tuberculosis*), each subunit adopts a TIM barrel-like fold with α -helices surrounding a central barrel which is composed of eight parallel β -strands [Baca et al., 2000]. The subunit one of DHPS of *M. leprae* is 284 amino acids in length and is encoded by *folp1* gene [Nopponpunth et al., 1999].

The presence of point mutations within *folp1* gene that encode DHPS was considered as the exclusive basis for molecular detection of dapsone resistance in leprosy. However, the detection of point mutations is an indication of resistance that should be correlated with the structural and functional changes they induce in the protein and ultimately with the clinical outcomes of treatment. The actual downstream functional implications of these point mutations in terms of the changes that they induce in the protein structure and function was scarcely studied. All the point mutations identified within the *M. leprae folp1* gene were non-synonymous as they induce an amino acid change in the encoded DHPS thereby leading to the structural variations and alterations in the drug interactions, making *M. leprae* resistant to dapsone [Rao and Kumar, 2008]. Point mutations that dictate drug resistance to dapsone, rifampicin, and ofloxacin in leprosy are identified through PCR and DNA sequencing, and the resistance outcome have been validated in the mouse foot pad and various other surrogate genetic studies [Williams et al., 2000; Sekar et al., 2011; Lavania et al., 2014; Vedithi et al., 2014]. The functional implications of these point mutations within active drug interacting genes include single amino acid changes in the peptide chains of the encoded proteins which may alter the protein loops and side chain interactions and thereby orientations of the active drug binding pockets in proteins [Vats et al., 2015]. This consequently result in the loss of drug interactions leading to development of resistance [Baca et al., 2000]. Although the analysis reveals preliminary information on the loss of interactions, it is important that the findings of this in-silico analysis further needs to be correlated with clinical outcomes of the disease to establish the functional impact of point mutations on drug resistance.

Molecular studies on drug resistance in mycobacteria with reference to sulfonamides indicated a loss in structural interaction with the target proteins [Baca et al., 2000]. A possible contribution of point mutations to the loss in interaction has been described in

earlier studies in various bacterial models [Maus et al., 2004; Silva et al., 2011]. This further led to the functional analysis of these point mutations in surrogate genetic studies [Nakata et al., 2011].

In this study, we used bioinformatics tools to understand the effect of known and reported point mutations in *folp1* gene [Nakata et al., 2011] which cause resistance to dapsone in leprosy. Molecular docking experiments were performed with dapsone and the corresponding native and mutated DHPS to identify the changes in the interaction energies, docking scores, binding pocket geometry, and hydrogen bonding patterns.

MATERIALS AND METHODS

SELECTION OF POINT MUTATIONS

The point mutations within *folp1* gene that cause amino acid changes in the DHPS are chosen from the literature and selected as shown in (Table I). Only the mutations that cause major changes in terms of loss of bacterial viability in MFP assays and have high levels of MIC (minimum inhibitory constants) of the drugs [Matsuoka et al., 2007; Nakata et al., 2011] in the surrogate mouse foot pad and genetic studies were selected for molecular docking analysis.

BIOINFORMATICS ANALYSIS

Schrodinger Suite 2014-3 containing the Maestro 9.9.013 was used as the working interface with DHPS as well as with dapsone. Additional modules in Schrödinger Release 2014-3 include Prime - version 3.7, LigPrep - version 3.1, and SiteMap - version 3.2 (Schrödinger, LLC, New York, NY, 2014). In the Small-Molecule Drug Discovery Suite 2014-3: Glide -version 6.4 (Schrödinger, LLC, New York, NY, 2014) was also used in the experimental procedures. Molecular preparation and docking experiments were performed as individual projects for dapsone and its corresponding native and mutant DHPS targets, in Maestro.

PREPARATION OF LIGAND

Structure Data File (SDF) for dapsone was downloaded from Pubchem Substances database of NCBI (SID: 134337927) and then was optimized for the docking experiments using LIGPREP [Chen and Foloppe, 2010]. OPLS2005 force field was used and structure was imported into LIGPREP panel in SDF format [Beard et al., 2013]. Hydrogen atoms were added in a manner consistent with the OPLS2005 and co-factors were removed from the structure using the "desalt" option. The ionization states were generated for the structure in a pH range of 7.0 ± 2.0 using "EPIK" submodule [Shelley et al., 2007]. The metal binding states were not added to DHPS. All possible tautomeric states were also generated using "generate tautomer" option. The stereoisomers were computed while retaining

TABLE I. Point mutations within *M. leprae* DHPS

Serial No.	Mutations	References
1	Thr53Ile	Nakata et al. [2011]
2	Thr53Ala	
3	Thr53Val	Matsuoka et al. [2007]
4	Pro55Arg	Nakata et al. [2011]
5	Pro55Leu	

the input chiralities of the structure. One low energy ring conformation was generated. The processed LIGPREP output file is taken into Maestro interface.

PROTEIN MODELING, REFINEMENT, AND ENERGY MINIMIZATION

PRIME Version 3.7.013 was used in the protein modelling and refinement experiments. The below procedure has been performed for native as well as the mutant DHPS. The mutations were incorporated by directly editing the native amino acid sequence at the sites specified in Table I and then homology modelling and refinements were performed. Native and each of the mutations were stored as different working projects in Maestro interface.

Homology modeling. The 284 amino acid sequence for *M. leprae* DHPS (Genbank ID: CAC29732.1) was taken from NCBI protein database. On the PRIME Homology Modeling panel, the sequence was entered in the text and PSI BLAST (Position-Specific Iterated-Basic Local Alignment Search Tool) homology search was performed taking non-redundant protein sequence database of NCBI as default, to identify structure templates [Nayeem et al., 2006]. The chain A of the “1.7 angstrom resolution crystal structure of DHPS from *M. tuberculosis* which is in complex with 6-hydroxymethylpterin monophosphate” (PDB ID: 1EYE) [Kshitija Iyer, 2014] was chosen as the template based on the identity of 77%, 86% of positives and 1% of gaps. The template was then aligned to the query sequence of 284 amino acids using CLUSTALW. Later knowledge based model building was performed without the inclusion of co-crystallized ligands or co-factors as dapson is absent in the co-crystallized ligands.

The structures were then brought into the Maestro interface wherein they were further refined and energy minimized. The homology model that was built was initially analyzed for the steric clashes which revealed clashes within distance less than that of the minimum allowed distances for all the amino acids. These clashes were removed on energy minimization. The Ramachandran plot revealed that only 2% of the amino acids (Ala57, Gly23, Gly92, Gly42, and Gly217) were found to be out of the favorable region. The amino acid sequence of the developed model was renumbered in “Multiple Sequence Editor Panel” where start point is set to “5” in order to match the order and numbering in the query sequence. A nick in the loop between amino acid numbers Ile58 and Ser59 was joined by the introduction of peptide bond and then the structure was refined. The hydrogen atoms were added in consistency with OPLS2005 force field parameters [Srinivasan et al., 2014] and protein reports were analyzed before refinement.

Refinement. The non-template loop that lies between amino acid numbers Gly50–Ala57 was refined using PRIME refinement panel [Zhu et al., 2014]. The variable-dielectric generalized Born – solvation model was used and extended serial loop sampling method was performed to orient the non-template loops. Then the amino acid residues that line the potential ligand binding region were identified using SITEMAP with default parameters. This was followed by refinement and prediction of missing side chains of the amino acids that line the ligand binding region using “Predict Side Chain” Panel in PRIME [Vijayakumar et al., 2014]. All the amino acid residues that were identified by the SITEMAP which lie within the ligand interacting region were chosen from the project table and were used in the side chain refinement.

Energy minimization. The refined protein structure was energy minimized using “Minimize” panel of PRIME. The entire protein structure was minimized with respect to its coordinates [Rapp et al., 2011]. Hundred cycles each of Truncated Newton and Conjugant gradient algorithms were used in the minimization. The energy minimization was performed to remove the steric clashes which were confirmed in the protein report. This minimized structure was used for molecular docking experiments.

MOLECULAR DOCKING EXPERIMENTS USING GLIDE

Receptor grid generation. The flexible hydroxyl groups within the ligand binding region of DHPS were represented on a grid by several different sets of fields that provided progressively more accurate scoring of the ligand poses. This was achieved by receptor grid generation panel in GLIDE. The molecules in the centroid of the workspace was taken for grid generation supposing that the docking ligand is confined to the enclosing box [Kawatkar et al., 2009].

GLIDE extra-precision docking. Extra-precision flexible docking was performed between dapson and DHPS with permissible nitrogen inversions and ring confirmations. The GLIDE docking scores and penalties were recorded [Friesner et al., 2006].

Energy minimization of docked model. The docked model was energy minimized again by PRIME. This was performed to orient the ligand in the lowest energy confirmation while retaining interactions with the receptor [Lyne et al., 2006].

Energy calculations. The binding energy variations were recorded using PRIME MM-GBSA panel. The PRIME MM-GBSA panel was used to calculate ligand binding energies and ligand strain energies for the ligands and receptor, using MM-GBSA technology available with PRIME [Vijayakumar et al., 2014].

Binding pocket dimensions. The active site/binding pocket dimensions of dapson on DHPS was calculated using CASTp (Computed atlas of surface topology of proteins) server [Dundas et al., 2006]. CASTp program uses solvent probes of sphere radius of 1.4 Å into the concavities in the receptor. The computational geometry that was applied in the current calculation includes Delaunay triangulation and alpha complex based shape measurement. The advantages include the following: (i) pockets and cavities are identified analytically, (ii) the boundary between the bulk solvent and the pocket is defined precisely, and (iii) all calculated parameters are rotationally invariant, and do not involve

TABLE II. Binding Pocket/Cavity Measurements Using CASTp for Native and Mutant DHPS (Area and Volume is Expressed in Angstrom Units)

Serial No.	Native/mutant DHPS	Area of the active binding pocket	Volume of the binding pocket
1	Native	73 Å ²	60.7 Å ³
2	Thr53Ala	255.4 Å ²	233.6 Å ³
3	Thr53Ile	472.6 Å ²	659.9 Å ³
4	Thr53Val	371.9 Å ²	400 Å ³
5	Pro55Arg	393 Å ²	385 Å ³
6	Pro55Leu	116 Å ²	210 Å ³

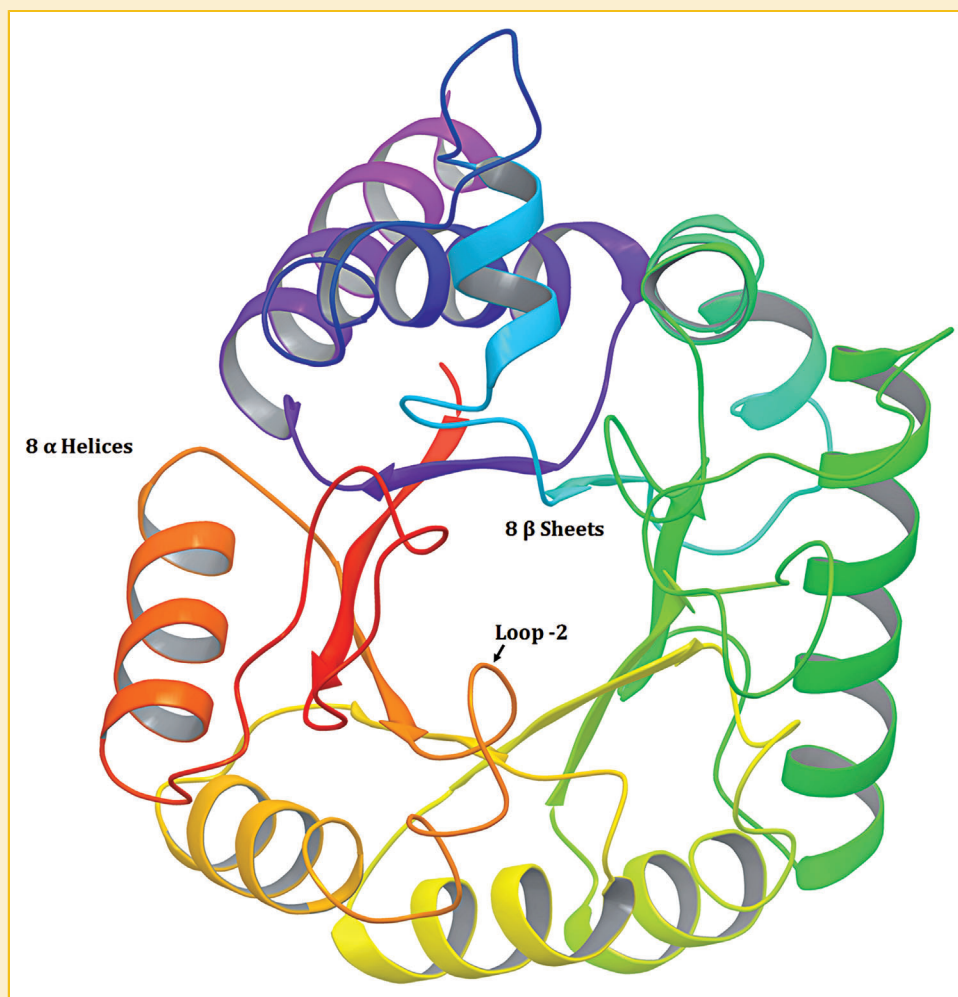


Fig. 1. Native structure of DHPS of *M. leprae*. The structure resembles a Tim Barrel-like fold with eight α helices and eight β sheets in the center adjacent to the dapsone binding pocket. The non-template loop (Loop 2) was highlighted.

discretization and they make no use of dot surface or grid points. The application provides information about the accessible areas on the surface and also the inaccessible areas in the deep cavities. The results included area and volume (solvent accessible and Molecular surfaces) of the binding cavities and also the circumference of the mouth of the binding pocket. In the current calculations, the measuring parameters were left to default where a value of 1.4 Å was used as the probe radius [Vats et al., 2015]. The docked structures were submitted in PDB format and the results were displayed in Jmol format.

RESULTS

The changes in the dapsone interaction with *M. leprae* DHPS was analyzed in terms of changes in the hydrogen and hydrophobic bonds, interaction energies, volume and orientation of the binding pocket, and docking scores.

VARIATIONS IN THE GEOMETRIC MEASUREMENTS OF THE BINDING POCKET/CAVITY ACROSS THE NATIVE/MUTANT DHPS

The native and mutant docked PDB files were analyzed for the binding cavity geometry in terms of area and volume which revealed an increase in the area and volume of binding pocket in the mutant proteins when compared to the native protein (Table II). This increase in the volume of the binding pocket in all mutant DHPS forms when compared to the native form can affect the binding of dapsone at the active site of DHPS in mutant proteins and also destabilizes the ligand in the active site. The observation were further validated by changes in the bonding patterns and interaction energies.

Homology model of native *M. leprae* DHPS and dapsone interaction. The generated homology model of *M. leprae* DHPS revealed a TIM barrel-like fold with eight α -helices surrounding the eight β -strands. The β strands line the active site of the enzyme and contains a total of seven loops in the structure (Fig. 1). Of all the loops, loop 2 remains as a loop of interest as all the known mutations in *M. leprae* DHPS lie within this loop encompassing the residues

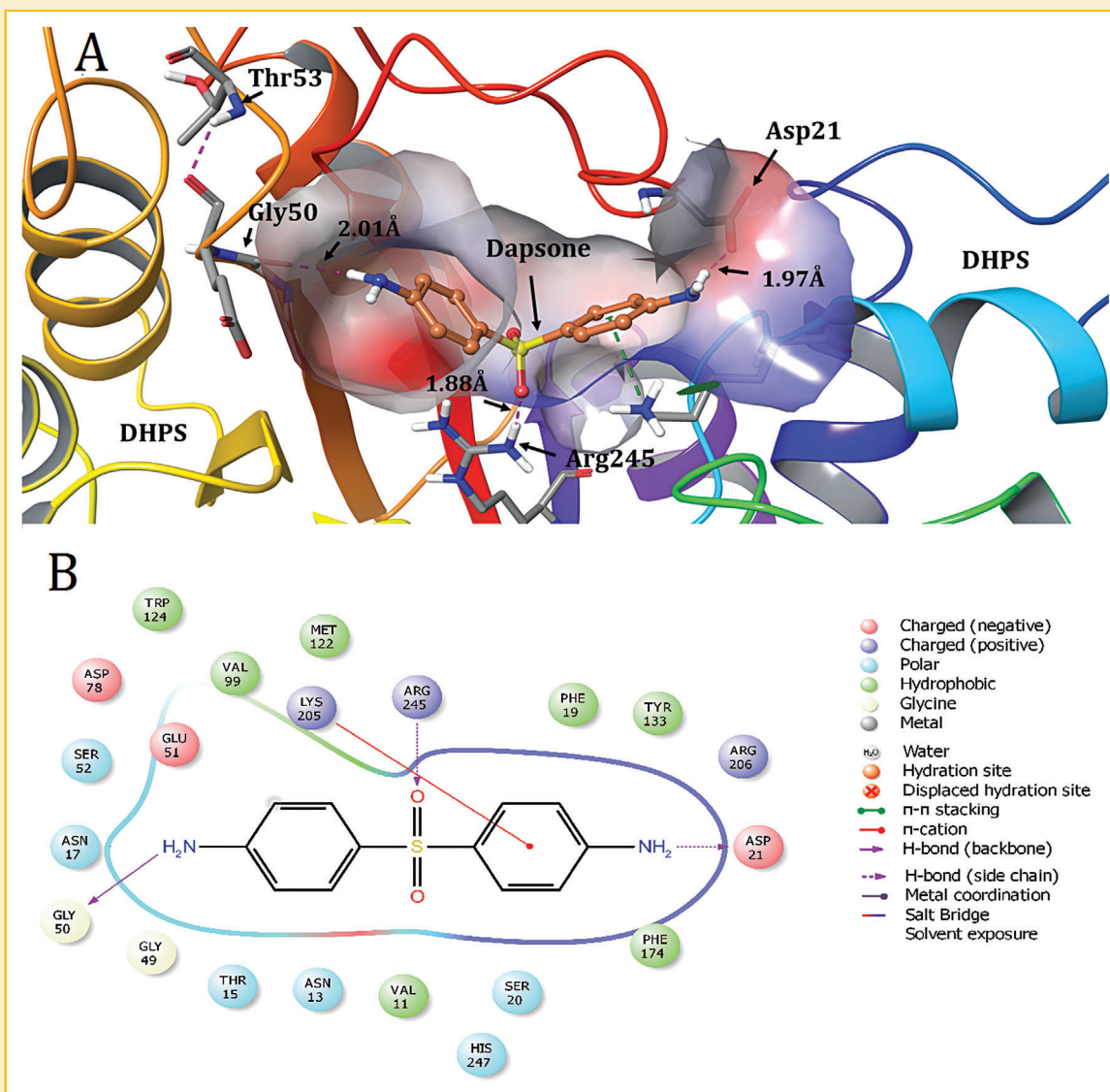


Fig. 2. A: Dapsone (Amber) was positioned in the interacting pocket of DHPS with hydrogen bonds (dotted lines in Magenta). The Thr53 was displayed to demonstrate its role in forming hydrogen bonds with Glu51 which is conjoint with Gly50. The hydrogen bonds are represented in pink dotted lines with the appropriate bond lengths in angstrom (Å) units. B: Interaction map of Dapsone with native DHPS showing hydrogen bonding. The pocket encompasses three negatively charged (red) and three positively charged (violet) amino acid residues besides seven hydrophobic (green) and six polar (blue) amino acid residues. Two glycine molecules are also present in the interaction map. Lysine at position 205 forms a cationic bridge. The dotted lines (pink) indicate side chain hydrogen bonds and arrows (pink) indicate main chain hydrogen bonds.

ranging from amino acid positions 48–60. This loop remained as a non-template loop as there is only 75% sequence identity with loop 2 of 1EYE. The channel where the active binding site lies is defined by the docking experiments which revealed the contributing amino acids as Val 11, Asn13, Thr15, Asn17, Phe19, Ser20, and Asp 21 from loop 1, Gly 49, Gly50, Glu51, and Ser52 from loop2, Asp78 and Val99 from loop 3, Trp124 and Met122 from loop 4, Tyr133 from loop 5, Phe174 from loop 6 and Lys 205, His247 and Arg245 from loop 7. It was observed that with the current docking parameters, dapsone forms three hydrogen bonds with DHPS which include bonding with main chain oxygen atom of Gly50 with the bond length of 2.01 Å, side chain nitrogen atoms of Arg245 with a bond length of 1.88 Å, and with side chain oxygen atom of Asn21 with a

bond length of 1.97 Å (Fig. 2A). These bonds stabilize the structure of dapsone in the interacting pocket of DHPS and all the amino acids that line the interacting pocket are shown in (Fig. 2B). The main chain hydrogen bond formed with Gly50 was found to be stable in the native form but this bond was not observed in the mutant forms. The position of Gly50 was stabilized by the intra-residual hydrogen bonds between Gly50, Glu51, and Thr53. The Thr53 acts as an anchoring residue to hold the Gly50 in position. This was observed in the native docked structure in contrast to the mutants Ile53, Val53, and Ala53. Feeble intermolecular interactions like hydrophobic interactions and hydrogen bond formation are very critical for stabilizing the energetically favored ligands, in an open conformational environment of protein structures. We have also noted the

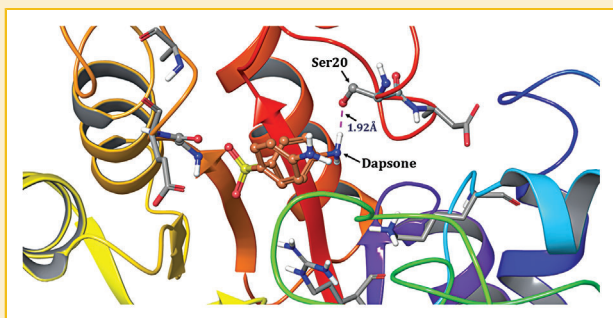


Fig. 3. Hydrogen bond interactions with Thr53Ala DHPS mutant.

number of hydrophobic, polar, and charged (negative and positive) interactions specifically in the interaction maps (Fig. 2B). This image displays hydrogen bonds and seven hydrophobic residues.

The docking parameter revealed a score based on the extra-precision (XP) docking that was performed with Glide. This docking score along with the docking (Glide) energy, Van der waals energy, electrostatic energy, and binding energy trend between native and mutant docked structures which was further validated using Molecular Mechanics/Generalized Born Surface Area (MM GBSA) Technology, were documented [Hou et al., 2011]. This technology employs a generalized born model and solvent accessibility method to elicit free energies from structural information circumventing the need for complex computational free energy simulations [Tuffery and Derreumaux, 2011]. The docking of dapson with native DHPS revealed a docking score of -4.48 Kcal/mol with a Glide energy, Van der waals energy, and electrostatic energy of -35.88 , -25.54 , and -10.35 Kcal/mol, respectively. The PRIME MMGBSA ΔG is calculated to be -51.92 Kcal/mol using the above mentioned technology. The energy changes in the native as well as the mutant DHPS were summarized along with the description of the measured parameters in (Table III).

MUTANT DHPS AND DAPSONE INTERACTION

(a) **Thr53Ala:** A mutation at position 53 in the sequence where threonine is replaced with alanine was induced in the native sequence and model development, refinement and energy minimizations were performed similarly to that of the native model. In this mutant structure, dapson formed only one hydrogen bond with side chain oxygen atom of Ser20 with a bond length of 1.92\AA (Fig. 3) however, Glu51, Gly50 and Ser52 remained in the interaction loop. The hydrophobic interactions were also reduced to five amino acid residues (Fig. 8A) in the

mutant when compared to the native DHPS. These changes in the hydrogen bonding render the dapson interaction frailer when compared to the native docking which was also reflected in the energy changes where the overall docking score was reduced to -4.10 Kcal/mol with a Glide energy, Van der waals energy, and electrostatic energy of -32.14 , -23.76 , and -5.37 Kcal/mol, respectively. The PRIME MMGBSA ΔG was reduced to 35.65 Kcal/mol when compared to the native DHPS indicating a decrease in the interaction of dapson with Thr53Ala mutant of DHPS. These energy changes and changes in interaction are concomitant with the increase in volume of the binding pocket to 233.6\AA^3 when compared to 60.7\AA^3 in the native structure.

- (b) **Thr53Ile:** In this mutation, threonine at amino acid position 53 was replaced by isoleucine. The interaction revealed that dapson formed three hydrogen bonds, one with side chain hydrogen atom of Asn17 at a bond length of 2.31\AA , one with main chain oxygen atom of Gly23 at a bond length of 1.93\AA , and one with the main chain oxygen atom of Gly173 at a bond length of 2.42\AA (Fig. 4). The hydrophobic interactions involve six amino acid residues and Ile53 was one among the interacting residues which was absent in the native interactions. This was reflected in the interaction map of the docking (Fig. 8B). These docking changes or weakening of the interaction was further observed in the energy changes where the overall docking score was reduced to -3.55 Kcal/mol with a Glide energy, Van der waals energy, and electrostatic energy of -30.85 , -21.15 , and -3.69 Kcal/mol, respectively. The PRIME MMGBSA ΔG was reduced to 35.24 Kcal/mol when compared to the native DHPS rendering a weak interaction and destabilization of the ligand in the active site. Consistently, due to the increase in energy change, the volume increase was maximum in this mutant with 659.9\AA^3 . Orientation of the interaction loops demonstrated major changes in this mutant leading to the analogous increase in the volume of the binding pocket.
- (c) **Thr53Val:** Similar replacement with valine at position 53 was characterized by changes in the bonding interactions especially in the hydrogen bonds where dapson formed three hydrogen bonds, one with the main chain oxygen atom of Tyr133 with the bond length of 2.06\AA , main chain oxygen atom of Lys176 with the bond length of 1.97\AA , and main chain hydrogen atom of Arg206 with the bond length of 1.81\AA (Fig. 5). The hydrophobic interactions were reduced to three residues making the interaction weak (Fig. 8C) which was also noted in the dropping of interaction energies where the overall docking score was reduced to -2.85 Kcal/mol with Glide energy, Van der waals energy, and electrostatic energy of -26.76 , -19.68 , and -5.09 Kcal/mol, respectively. The PRIME MMGBSA ΔG was reduced to 46.49 Kcal/mol when compared to the native DHPS. The energy change was maximum in this mutant and concomitantly the volume of the binding pocket increased to 400\AA^3 .

TABLE III. Docking Score and Interaction Energy Differences for Molecular Docking of Dapson With Native and Mutant DHPS

Measuring parameter	Description	Energy changes in Kcal/mol					
		Native	Thr53Ala	Thr53Ile	Thr53Val	Pro55Arg	Pro55Leu
XP GScore	Total GlideScore	-4.48	-4.10	-3.55	-2.85	-4.19	-3.26
Glide energy	Modified Coulomb-van der Waals interaction energy	-35.88	-32.14	-30.85	-26.76	-29.65	-26.45
Glide evdw	Van der Waals energy	-25.54	-23.76	-21.15	-19.68	-24.48	-20.89
Glide ecoul	Electrostatic energy	-10.35	-5.37	-3.69	-5.09	-5.17	-5.55
MMGBSA dG bind	Total binding energy calculated by MM GBSA technology	-51.92	-35.64	-35.24	-46.47	-47.69	-41.36

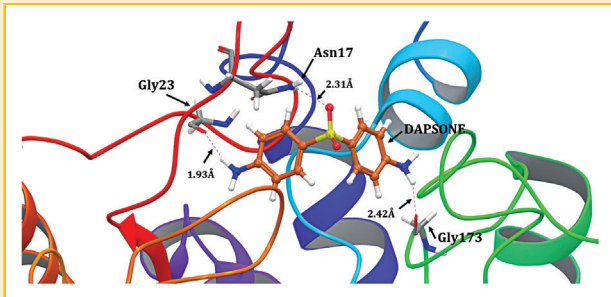


Fig. 4. Hydrogen bond interactions with Thr53Ile DHPS mutant.

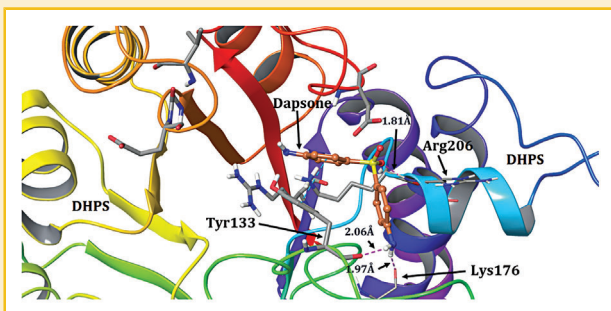


Fig. 5. Hydrogen bond interactions with Thr53Val DHPS mutant.

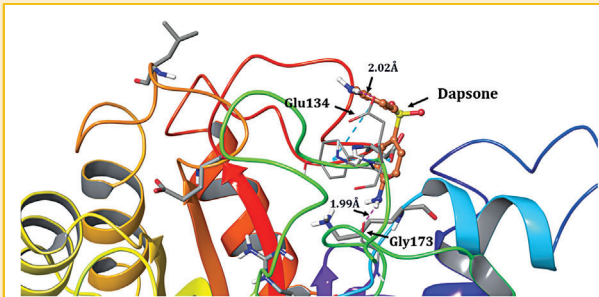


Fig. 7. Hydrogen bond interactions with Pro55Leu DHPS mutant.

(d) **Pro55Arg:** This mutation involves replacement of proline at the amino acid position 55 with arginine. This mutation was induced in the sequence by the same procedure that was applied to the mutations at position 53. The model development, structure refinement, and energy minimizations were performed in a similar fashion as that of the native DHPS model. Dapsone formed five hydrogen bonds in which two main chain bonds were formed with oxygen atoms of Gly50 with the bond length of 1.94 Å and Phe19 with the bond length of 2.50 Å, and side chain hydrogen bonds with oxygen atoms of Glu51 at a bond length of 2.11 Å, hydrogen atom of Arg245 with the bond length of 1.8 Å, and oxygen atom of Asp21 with the bond length of 1.93 Å (Fig. 6). The hydrogen bonds contribute to the stability of the ligand, however, the interaction was weakened in the hydrophobic

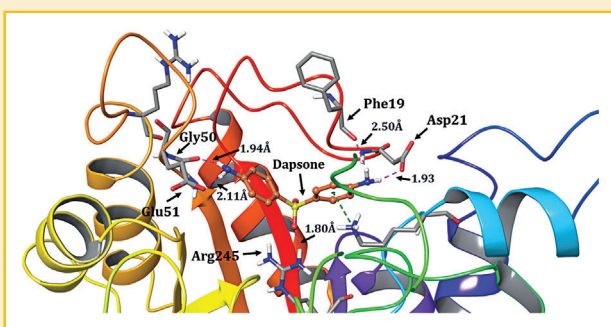


Fig. 6. Hydrogen bond interactions with Pro55Arg DHPS mutant.

contacts as only four amino acid residues contributed (Fig. 8D). The energy changes reveal overall docking score of -4.19 Kcal/mol and Glide energy, Van der waals energy, and electrostatic energy of -29.65 , -24.48 , and -5.17 Kcal/mol, respectively. The PRIME MMGBSA ΔG was reduced to 47.69 Kcal/mol when compared to the energy changes in the native DHPS model. Although the energy change is minimum in this model, the distinctive cyclic structure of proline's side chain affects the rate of peptide bond formation between proline and other amino acids making the conformation more rigid. The conformation and amino acid interactions are lost when arginine, which contains 3-carbon aliphatic straight chain, replaces proline. This structural change may induce an increase in the hydrogen bond formation and delocalization of the positive charge. These changes possibly impact the loop orientations in the binding pocket leading to an increase in the volume to 385 \AA^3 .

(e) **Pro55Leu:** Point mutation at the amino acid position 55 where proline is replaced by leucine in DHPS causes changes in the dapsone interaction where only two hydrogen bonds were formed, one with main chain oxygen atom of Gly173 with a bond length of 1.99 Å and one with the side chain oxygen atom of Glu134 with a bond length of 2.02 Å (Fig. 7). The analysis of hydrophobic interactions revealed the association of four amino acids when compared to seven in the native DHPS (Fig. 8E). This change in the bonding pattern and hydrophobic interactions were further reflected in the energy changes where the overall docking score is -3.26 Kcal/mol; with Glide energy, Van der waals energy, and electrostatic energy of -26.45 , -20.89 , and -5.55 Kcal/mol, respectively. The PRIME MMGBSA ΔG was reduced to 41.36 Kcal/mol when compared to the energy changes in the native DHPS model. Leucine possesses a nonlinear aliphatic side chain which plays a pivotal role in the modulation of Van der waals interactions. These changes in interactions being weak has possibly led to a minimal increase in the volume of the binding pocket to 210 \AA^3 when compared to the other mutant structures.

DISCUSSION

The presence of point mutations with the *folp1* gene of *M. leprae* were identified in 1999 [Kai et al., 1999] and they remained in highly conserved amino acid codon positions 53 and 55 of the *M. leprae* DHPS. These mutations play a role in conferring sulfonamide

M. tuberculosis DHPS provided insights on the structural interaction of DHPS with sulfonamides [Rao and Kumar, 2008]; however, no studies were performed through docking experiments involving *M. leprae* DHPS to understand the downstream functional implications of the point mutations on the outcome of dapson resistance in leprosy. Dapsone is known to competitively inhibit DHPS as it competes with pABA on the active site.

In the current study, we developed homology model for *M. leprae* DHPS and it was observed that both the mutations (positions 53 and 55) lie very close to the active site for dapson interaction as observed similarly in crystal structure of *M. tuberculosis* DHPS [Baca et al., 2000]. We also observed that Thr53 forms intra-residual hydrogen bonds with Gly50 and Glu51 that interacts with dapson in the native DHPS and hence stabilizes the ligand interaction. These bonds were absent in the mutant forms. The changes in the geometry of the binding pockets/cavities were well characterized in various studies where point mutations at specific positions were involved [Vats et al., 2015]. The increase in volume of the binding cavity of the receptor in the mutant DHPS proteins reveals a weak interaction and destabilization of the ligands, similar to that observed in the other studies [Farmer et al., 2010; Chowdhury et al., 2014]. Our results indicated a three- to four fold increase in the volume of the binding cavity in mutant DHPS when compared to the native forms. This increase in volume can be a possible reason for the weak interactions of dapson and the resulting resistance.

In most of the protein-ligand interactions, the hydrophobic and hydrogen bond interactions play a major role in the stabilized interaction of ligands [Patil et al., 2010]. In the current study, we have noted changes in the hydrogen bond patterns and a prominent decrease in the hydrophobic interactions in the mutant DHPS forms when compared to that of the native form. This has induced an equivalent effect on the interaction energy changes as stated in Table III. The hydrogen and polar interactions with residues of loop 2 which were present in the native docked model were retained in only one mutant form, that is, Pro55Arg while all the other mutants demonstrated weak or no interactions with the residues of loop 2.

The major impact of the point mutations in conferring resistance to a particular drug target include loss in interaction energy. In the Extra-Precision flexible docking of ligands and receptors using Glide, the total energy changes were calculated precisely with all possible orientations of the energy minimized, docked complexes [Tripathi et al., 2013]. We identified significant changes in the docking score, Glide energy, Van der waals energy, and electrostatic energy between the mutant models of DHPS when compared to the native model. Of all the five studied mutations, the Thr53Ile, Thr53Val, and Pro55Leu had low docking scores when compared to the native docked model. This was found to be consistent with the other energy changes such as the Glide energy, Van der waals energy, and the electrostatic energy which also remained low in these three mutant models when compared to the native model. However, all the mutant forms demonstrated a noted decrease in the interaction energies as measured through Glide. The loss in binding energy due to the presence of point mutations in drug interacting targets were also studied for rifampicin interactions with RNA polymerase β subunit in *M. leprae* [Vedithi et al., 2014; Nisha and Shanthi, 2015].

One of the limitations of this study is that the molecular dynamic simulations were not performed to identify all possible orientations of the ligand in the binding cavity of the receptor and computation of free energy changes, however, this need was circumvented to an extent by the use of PRIME MMGBSA based model for calculation of energy changes and binding affinities between dapson and *M. leprae* DHPS. This model of ΔG (free energy of binding/binding affinity) calculation showed significant correlation between calculated and experimental binding affinities between a diverse set of proteins and their corresponding ligands [Greenidge et al., 2013]. The formulation simply subtracts the free energy of the protein (P) and the ligand (L) from the free energy of the protein ligand (PL) complex; however, the free energy of the three molecular systems P, L, and PL is calculated taking into account the total molecular mechanics energy of the molecular system in the gas phase, a correction for solvation free energy and the entropy of the system [Hayes et al., 2011]. We have noted a significant decrease in the total free energy of binding between the native and the mutant forms of DHPS where the values were reduced to a much higher extent in the Thr53Ile and Thr53Val mutants (Table III). These observations were in correlation with the minimum inhibitory constant of dapson that is required for the inhibition of these mutant DHPS targets in the in-vitro experiments [Nakata et al., 2011].

In conclusion, our study is a pivotal attempt to design the homology models for the native and mutant structures of DHPS of *M. leprae* and to study the variations in dapson interaction with both the forms, providing insights into need for identification of novel and potential drug targets to combat dapson resistant leprosy. The energy changes and changes in the bonding patterns revealed the structural and mechanistic effects of these mutations on inducing dapson resistance in leprosy.

ACKNOWLEDGMENTS

The authors would like to thank all the administrative and laboratory staff of The Schieffelin Institute of Health-Research and Leprosy Center (Karigiri) who are involved in the collection and analysis of the data and literature. We extend our special thanks to Dr. Lakshmi Rajan who provided technical and literature insights and also to Dr. Richard for suggestions on the preparation of the manuscript. Our gratitude to all the technical and resource personnel at the Schrodinger, Inc. (Bangalore) for their provision of software and excellent application support in using Schrodinger Suite 2014-3.

REFERENCES

- Baca AM, Sirawaraporn R, Turley S, Sirawaraporn W, Hol WG. 2000. Crystal structure of *Mycobacterium tuberculosis* 7,8-dihydropteroate synthase in complex with pterin monophosphate: New insight into the enzymatic mechanism and sulfa-drug action. *J Mol Biol* 302:1193–1212.
- Beard H, Cholleti A, Pearlman D, Sherman W, Loving KA. 2013. Applying physics-based scoring to calculate free energies of binding for single amino acid mutations in protein-protein complexes. *PLoS ONE* 8:e82849.
- Bullock WE. 1983. Rifampin in the treatment of leprosy. *Rev Infect Dis* 5: S606–S613.
- Cambau E, Carthagena L, Chauffour A, Ji B, Jarlier V. 2006. Dihydropteroate synthase mutations in the *folP1* gene predict dapson resistance in relapsed cases of leprosy. *Clin Infect Dis* 42:238–241.

- Chen I-J, Foloppe N. 2010. Drug-like bioactive structures and conformational coverage with the LigPrep/ConfGen suite: Comparison to programs MOE and catalyst. *J Chem Inf Model* 50:822–839.
- Chowdhury MRH, Bhuiyan MI, Saha A, Mosleh IM, Mondol S, Ahmed CMS. 2014. Identification and analysis of potential targets in *Streptococcus sanguinis* using computer aided protein data analysis. *Adv Appl Bioinforma Chem AABC* 7:45–54.
- Desikan KV. 2012. Elimination of leprosy & possibility of eradication—The Indian scenario. *Indian J Med Res* 135:3–5.
- Dundas J, Ouyang Z, Tseng J, Binkowski A, Turpaz Y, Liang J. 2006. CASTp: Computed atlas of surface topography of proteins with structural and topographical mapping of functionally annotated residues. *Nucleic Acids Res* 34:W116–W118.
- Farmer R, Gautam B, Singh S, Yadav PK, Jain PA. 2010. Virtual screening of AmpC/β-lactamase as target for antimicrobial resistance in *Pseudomonas aeruginosa*. *Bioinformatics* 4:290–294.
- Friedmann PS. 1973. Dapsone-resistant leprosy. *Proc R Soc Med* 66:623–624.
- Friesner RA, Murphy RB, Repasky MP, Frye LL, Greenwood JR, Halgren TA, Sanschagrin PC, Mainz DT. 2006. Extra precision glide: Docking and scoring incorporating a model of hydrophobic enclosure for protein-ligand complexes. *J Med Chem* 49:6177–6196.
- Greenidge PA, Kramer C, Mozziconacci J-C, Wolf RM. 2013. MM/GBSA binding energy prediction on the PDBbind data set: Successes, failures, and directions for further improvement. *J Chem Inf Model* 53:201–209.
- Hayes JM, Skamnaki VT, Archontis G, Lamprakis C, Sarrou J, Bischler N, Skaltsounis A-L, Zographos SE, Oikonomakos NG. 2011. Kinetics, *in silico* docking, molecular dynamics, and MM-GBSA binding studies on prototype indirubins, KT5720, and staurosporine as phosphorylase kinase ATP-binding site inhibitors: The role of water molecules examined. *Proteins* 79:703–719.
- Hou T, Wang J, Li Y, Wang W. 2011. Assessing the performance of the molecular mechanics/Poisson Boltzmann surface area and molecular mechanics/generalized Born surface area methods. II. The accuracy of ranking poses generated from docking. *J Comput Chem* 32:866–877.
- Ji B, Grosset J. 1991. Ofloxacin for the treatment of leprosy. *Acta Leprol* 7:321–326.
- Kai M, Matsuoka M, Nakata N, Maeda S, Gidoh M, Maeda Y, Hashimoto K, Kobayashi K, Kashiwabara Y. 1999. Diaminodiphenylsulfone resistance of *Mycobacterium leprae* due to mutations in the dihydropteroate synthase gene. *FEMS Microbiol Lett* 177:231–235.
- Kawatkar S, Wang H, Czereminski R, Joseph-McCarthy D. 2009. Virtual fragment screening: An exploration of various docking and scoring protocols for fragments using Glide. *J Comput Aided Mol Des* 23:527–539.
- Kshitija Iyer AK. 2014. Extraction of bioactive compounds from millingtonia hortensis for the treatment of dapsone resistance in leprosy. *J Microb Biochem Technol* R1:006. doi: 10.4172/1948-5948.R1-006
- Lavania M, Jadhav RS, Chaitanya VS, Turankar R, SelvaSekhar A, Das L, Darlong F, Hambroom U, Kumar S, Sengupta U. 2014. Trend in drug resistance pattern in *Mycobacterium leprae* isolates from the relapsed leprosy patients from The Leprosy Mission (TLM) Hospitals in India. *Lepr Rev* 85:177–185.
- Lyne PD, Lamb ML, Saeh JC. 2006. Accurate prediction of the relative potencies of members of a series of kinase inhibitors using molecular docking and MM-GBSA scoring. *J Med Chem* 49:4805–4808.
- Matsuoka M, Budiawan T, Aye KS, Kyaw K, Tan EV, Cruz ED, Gelber R, Saunderson P, Balagon V, Pannikar V. 2007. The frequency of drug resistance mutations in *Mycobacterium leprae* isolates in untreated and relapsed leprosy patients from Myanmar, Indonesia and the Philippines. *Lepr Rev* 78:343–352.
- Maus CE, Plikaytis BB, Shinnick TM. 2005. Mutation of tlyA confers capreomycin resistance in *Mycobacterium tuberculosis*. *Antimicrob Agents Chemother* 49:571–577.
- Nakata N, Kai M, Makino M. 2011. Mutation analysis of the *Mycobacterium leprae folP1* gene and Dapsone resistance. *Antimicrob Agents Chemother* 55:762–766.
- Nayeem A, Sitkoff D, Krystek S. 2006. A comparative study of available software for high-accuracy homology modeling: From sequence alignments to structural models. *Protein Sci Publ Protein Soc* 15:808–824.
- Nisha J, Shanthi V. 2015. Computational simulation techniques to understand rifampicin resistance mutation (S425L) of *rpoB* in *M. leprae*. *J Cell Biochem*. 2015 Feb 10. doi: 10.1002/jcb.25083
- Nopponpunnth V, Sirawaraporn W, Greene PJ, Santi DV. 1999. Cloning and expression of *Mycobacterium tuberculosis* and *Mycobacterium leprae* dihydropteroate synthase in *Escherichia coli*. *J Bacteriol* 181:6814–6821.
- Patil R, Das S, Stanley A, Yadav L, Sudhakar A, Varma AK. 2010. Optimized hydrophobic interactions and hydrogen bonding at the target-ligand interface leads the pathways of drug-designing. *PLoS ONE* 5:e12029.
- Rao GS, Kumar M. 2008. Structure-based design of a potent and selective small peptide inhibitor of *Mycobacterium tuberculosis* 6-hydroxymethyl-7, 8-dihydropteroate synthase: A computer modelling approach. *Chem Biol Drug Des* 71:540–545.
- Rapp C, Kalyanaraman C, Schiffmiller A, Schoenbrun EL, Jacobson MP. 2011. A molecular mechanics approach to modeling protein-ligand interactions: Relative binding affinities in congeneric series. *J Chem Inf Model* 51:2082–2089.
- Seydel JK, Richter M, Wempe E. 1980. Mechanism of action of the folate blocker diaminodiphenylsulfone (dapsone, DDS) studied *in E. coli* cell-free enzyme extracts in comparison to sulfonamides (SA). *Int J Lepr Mycobact Dis Off Organ Int Lepr Assoc* 48:18–29.
- Shelley JC, Cholleti A, Frye LL, Greenwood JR, Timlin MR, Uchimaya M. 2007. Epik: A software program for pK(a) prediction and protonation state generation for drug-like molecules. *J Comput Aided Mol Des* 21:681–691.
- Sekar B, Arunagiri K, Kumar BN, Narayanan S, Menaka K, Oommen PK. 2011. Detection of mutations in *folP1*, *rpoB* and *gyrA* genes of *M. leprae* by PCR-direct sequencing—A rapid tool for screening drug resistance in leprosy. *Lepr Rev* 82:36–45.
- Silva PEAD, Palomino JC. 2011. Molecular basis and mechanisms of drug resistance in *Mycobacterium tuberculosis*: Classical and new drugs. *J Antimicrob Chemother* 66:1417–1430.
- Srinivasan P, Chella Perumal P, Sudha A. 2014. Discovery of novel inhibitors for Nek6 protein through homology model assisted structure based virtual screening and molecular docking approaches. *Sci World J* 2014:e967873.
- Tripathi SK, Muttineni R, Singh SK. 2013. Extra precision docking, free energy calculation and molecular dynamics simulation studies of CDK2 inhibitors. *J Theor Biol* 334:87–100.
- Tuffery P, Derreumaux P. 2011. Flexibility and binding affinity in protein-ligand, protein-protein and multi-component protein interactions: Limitations of current computational approaches. *J R Soc*.
- Vats C, Dhanjal JK, Goyal S, Gupta A, Bharadvaja N, Grover A. 2015. Mechanistic analysis elucidating the relationship between Lys96 mutation in *Mycobacterium tuberculosis* pyrazinamidase enzyme and pyrazinamide susceptibility. *BMC Genomics* 16:S14.
- Vedithi SC, Lavania M, Kumar M, Kaur P, Turankar RP, Singh I, Nigam A, Sengupta U. 2014. A report of rifampin-resistant leprosy from northern and eastern India: Identification and *in-silico* analysis of molecular interactions. *Med Microbiol Immunol*. 2015 Apr;204(2):193–203. doi: 10.1007/s00430-014-0354-1. Epub 2014 Sep 9.
- Vijayakumar B, Parasuraman S, Raveendran R, Velmurugan D. 2014. Identification of natural inhibitors against angiotensin I converting enzyme for cardiac safety using induced fit docking and MM-GBSA studies. *Pharmacogn Mag* 10:S639–S644.
- Weekly Epidemiological Record (WER) - WHO | 5 September 2014, vol. 89, 36 (pp. 389–400). WHO.

Williams DL, Spring L, Harris E, Roche P, Gillis TP. 2000. Dihydropteroate synthase of *Mycobacterium leprae* and Dapsone resistance. *Antimicrob Agents Chemother* 44:1530-1537.

Zhu K, Day T, Warshaviak D, Murrett C, Friesner R, Pearlman D. 2014. Antibody structure determination using a combination of homology

modeling, energy-based refinement, and loop prediction. *Proteins Struct Funct Bioinforma* 82:1646-1655.

Zhu YI, Stiller MJ. 2001. Dapsone and sulfones in dermatology: Overview and update. *J Am Acad Dermatol* 45:420-434.